THE JOURNAL OF BIOLOGICAL CHEMISTRY VOL. 285, NO. 19, pp. 14389–14398, May 7, 2010

Glucose Suppression of Glucagon Secretion

*METABOLIC AND CALCIUM RESPONSES FROM α-CELLS IN INTACT MOUSE PANCREATIC ISLETS**

Received for publication, September 23, 2009, and in revised form, March 11, 2010 Published, JBC Papers in Press, March 15, 2010, DOI 10.1074/jbc.M109.069195

Sylvain J. Le Marchand and David W. Piston[1]

From the Department of Molecular Physiology and Biophysics, Vanderbilt University, Nashville, Tennessee 37232

Glucagon is released from α-cells present in intact pancreatic islets at glucose concentrations below 4 mM, whereas higher glucose levels inhibit its secretion. The mechanisms underlying the suppression of α-cell secretory activity are poorly understood, but two general types of models have been proposed as follows: direct inhibition by glucose or paracrine inhibition from non-α-cells within the islet of Langerhans. To identify α-cells for analysis, we utilized transgenic mice expressing fluorescent proteins targeted specifically to these cells. Measurements of glucagon secretion from pure populations of flow-sorted α-cells show that contrary to its effect on intact islets, glucose does stimulate glucagon secretion from isolated α-cells. This observation argues against a direct inhibition of glucagon secretion by glucose and supports the paracrine inhibition model. Imaging of cellular metabolism by two-photon excitation of NAD(P)H autofluorescence indicates that glucose is metabolized in α-cells and that glucokinase is the likely rate-limiting step in this process. Imaging calcium dynamics of α-cells in intact islets reveals that inhibiting concentrations of glucose increase the intracellular calcium concentration and the frequency of α-cell calcium oscillations. Application of candidate paracrine inhibitors leads to reduced glucagon secretion but did not decrease the α-cell calcium activity. Taken together, the data suggest that suppression occurs downstream from α-cell calcium signaling, presumably at the level of vesicle trafficking or exocytotic machinery.

Endocrine function of the islet of Langerhans is critical for the regulation of blood glucose homeostasis. Mouse islets are "micro-organs" composed of insulin-secreting β-cells (70–85% of the cells), glucagon-secreting α-cells (10–15%), along with other cell types (1, 2). Insulin and glucagon constitute a bi-hormonal system integral for maintaining normal blood glucose levels. Insulin lowers blood glucose by allowing tissues to absorb, metabolize, and store glucose. Glucagon, on the other hand, plays a protective role when blood glucose levels fall by stimulating hepatic glucose output via glycogenolysis and gluconeogenesis (3). Type 1 and late type 2 diabetes have been associated with elevated levels of glucagon that exacerbate the chronic hyperglycemia caused by insulin deficiency (4). Also, patients under treatment with insulin or insulin secretagogues often fail to secrete a sufficient amount of glucagon during hypoglycemic episodes (5). This reduced glucagon response increases the risk of severe iatrogenic hypoglycemia.

In normal physiology, glucagon secretion is maximal at low blood glucose levels (<4 mM), whereas higher glucose concentrations stimulate insulin release and reduce glucagon secretion. The cellular mechanisms leading to insulin secretion are fairly well understood. β-Cell glucose transporter (*i.e.* GLUT-2) and glucokinase ensure that glucose enters the glycolytic pathway (6–8). Glucose metabolism leads to an increase in ATP to ADP ratio that closes ATP-sensitive K^+ (K_{ATP}) channels (9, 10). The subsequent plasma membrane depolarization activates L-type voltage-gated calcium channels, and the resultant increase in cytoplasmic free calcium concentration ($[Ca^{2+}]_i$)[2] triggers exocytosis of insulin-containing vesicles (11–13). Similar to β-cells, α-cells contain the same secretory machinery as follows: glucose transporter (in this case GLUT-1), glucokinase, K_{ATP} channels, voltage-gated calcium channels (L-, T-, N-, and R-types) and secretory granules (14–19). Because of this similarity, one would naively expect increased glucagon release at elevated glucose concentrations. How glucose instead causes a suppression of glucagon secretion remains poorly understood. Proposed models for this suppression fall into two categories as follows: direct inhibition by glucose (17, 20, 21) and paracrine inhibition from non α-cells (*i.e.* insulin, zinc ions, or γ-aminobutyric acid (GABA) from β-cells (22–28) or somatostatin from δ-cells (29, 30)).

Research on α-cell function has been hindered by the lack of reliable methods to identify α-cells within intact pancreatic islets. Transgenic mice that specifically express fluorescent proteins in α-cells make it possible to distinguish them *in situ* (31, 32). Using islets from these animals, we were able to unequivocally investigate α-cell physiology within intact islets and from pure populations of flow-sorted α-cells. We found that α-cells retrieved from their intra-islet environment exhibit a greater basal glucagon secretion than α-cells in islets. Also, elevated concentrations of glucose (>12 mM) stimulate glucagon secretion from isolated α-cells, contrary to its effect on the islet. This opposite behavior supports a paracrine inhibition model where α-cell secretory activity would be dampened by other cell types within the islet. Fluorescence-based identification of α-cells is particularly well suited for laser-scanning microscopic approaches, which allows quantitative assess-

* This work was supported, in whole or in part, by National Institutes of Health Grants DK53434, GM72048, and RR25649.

[1] To whom correspondence should be addressed: 702 Light Hall, Vanderbilt University, 2215 Garland Ave., Nashville, TN 37232. Tel.: 615-322-7030; Fax: 615-322-7236; E-mail: dave.piston@vanderbilt.edu.

[2] The abbreviations used are: $[Ca^{2+}]_i$, cytoplasmic free calcium concentration; PBS, phosphate-buffered saline; GFP, green fluorescent protein; EYFP, enhanced yellow fluorescent protein; GABA, γ-aminobutyric acid; tdRFP, tandem dimer-red fluorescent protein; ANOVA, analysis of variance; FCCP, carbonyl cyanide *p*-trifluoromethoxyphenylhydrazone.

ments of glucose metabolism and intracellular calcium signals. We used two-photon excitation of the combined redox signal (33) from NADH and NADPH (referred to as NAD(P)H) to confirm that glucose is metabolized in α-cells. The NAD(P)H glucose dose-response curve indicates that glucokinase is the likely rate-limiting step in α-cell glucose metabolism. This metabolism is followed by an increase in islet α-cell intracellular calcium concentration and in the frequency of calcium oscillations, as measured by confocal fluorescence microscopy. These observations suggest that glucagon inhibition by glucose is not mediated by a decrease in calcium activity. Instead, glucagon suppression could involve a mechanism downstream from $[Ca^{2+}]_i$ signaling, presumably associated with the exocytotic machinery or granule trafficking.

EXPERIMENTAL PROCEDURES

Materials—Fluo4-AM, FuraRed-AM, propidium iodine, Accutase, fetal bovine serum, penicillin, streptomycin, Hanks' balanced salt solution, phosphate-buffered saline (PBS), and Roswell Park Memorial Institute (RPMI) 1640 medium were purchased from Invitrogen. Antibodies were purchased from Millipore (Billerica, MA). Unless specified, all other products were purchased from Sigma.

Transgenic Mice—All work with animals was conducted in compliance with the Vanderbilt University Institutional Animal Care and Use Committee (IACUC). Transgenic mice (C57BL/6 genetic background) that specifically express enhanced yellow fluorescent proteins (EYFP) in α-cells have been designed and described by Quoix *et al.* (32). Transgenic mice are identified by PCR on mouse tail DNA (Puregene mouse tail kit, Gentra Systems, Minneapolis, MN). EYFP-specific oligonucleotide primers are as follows: 5′-TGA CCC TGA AGT TCA TCT GCA CCA-3′ (forward) and 5′-TGT GGC GGA TCT TGA AGT TCA CCT-3′ (reverse), expected fragment size of 384 bp. Cre-specific primers are as follows: 5′-TGC CAC GAC CAA GTG ACA GC-3′ (forward) and 5′-CCA GGT TAC GGA TAT AGT TCA TG-3′ (reverse), expected size of 675 bp. The emission spectra of EYFP and Fluo4 overlap. We therefore use ROSA26 tandem dimer-red fluorescent protein (ROSA26-tdRFP) mice (34) obtained from the European Mouse Mutant Archive (EMMA, Munich, Germany) to perform Fluo4 imaging. GFP-labeled β-cells from transgenic MIP-GFP (Mouse Insulin Promoter-Green Fluorescent Protein) mice (35) were used for our NAD(P)H and FuraRed measurements on isolated β-cells.

Islet Isolation and Culture—Male mice (2–6-month-old) were anesthetized by intraperitoneal injection of 0.05 ml ketamine/xylazine (VedCo, St. Joseph, MO) at 80 and 20 mg/ml, respectively. We used a modified version of the collagenase digestion method described elsewhere (36). Islets were maintained in islet medium composed of RPMI 1640 medium supplemented with 10% fetal bovine serum, penicillin (100 units/ml), streptomycin (100 μg/ml), and glucose (11 mM) at 37 °C under 5% humidified CO_2. For imaging purposes, isolated islets were attached on gelatin (0.1%)-coated 35-mm glass-bottomed dishes (MatTek Corp., Ashland, MA).

Cell Dispersion and Cell Flow Sorting—~200 islets were extracted per pancreas and cultured overnight in suspension in islet medium. They were washed in PBS at pH 7.4 without calcium and magnesium chloride. Then they were digested in Accutase for 15 min at 37 °C (gentle shaking) and resuspended in imaging solution (*i.e.* filtered aqueous solution containing 125 mM NaCl, 5.7 mM KCl, 2.5 mM $CaCl_2$·2H2O, 1.2 mM $MgCl_2$, 10 mM HEPES, and 0.1% bovine serum albumin, pH 7.4) at 11 mM glucose. One to 2 h after Accutase dispersion, fluorescent cells were isolated by fluorescence-activated cell sorting. For this purpose, we used the BD FACSAria cell sorter (BD Biosciences) in the Vanderbilt Flow Sorting Core. EYFP, GFP, and propidium iodine (1 μg/ml) were excited at 488 nm; fluorescence was collected using a 500–560 bandpass filter for EYFP and GFP, and a 593–639 nm filter for propidium iodine. Doublet cells were discriminated by pulse geometry gating, looking at the area, height, and width of the voltage pulses. We were able to sort ~500 viable α-cells per pancreas. Purified β-cell populations were also prepared in a similar manner using islets from MIP-GFP mice (35).

Glucagon and Insulin Secretion Assays from Islets and Isolated α-Cells—Overnight cultured islets were preincubated for 1 h in basal imaging solution containing 1 mM glucose at 37 °C. Islets were placed into tubes (10 islets per tube) and exposed to different conditions at 37 °C for 1 h. Samples containing secreted hormones were analyzed by radioimmunoassays in the Vanderbilt Hormone Assay Core. Islet hormone content was measured after overnight freezing of the islets in 1% Triton X-100. Each measurement was duplicated. Hormone secretion was expressed as fractional release, *i.e.* the percentage of total hormone content released over a 1-h incubation period. α-Cells collected after flow sorting were resuspended and preincubated in imaging solution (1 mM glucose) for 1 h at 37 °C. α-Cells were then placed into tubes (50 α-cells per tube) and exposed to different conditions at 37 °C during 1 h.

Immunofluorescence—Islets were fixed in PBS containing 2% of paraformaldehyde for 20 min and permeabilized overnight at 4 °C in PBS with 0.3% Triton X-100, 5 mM sodium azide, 1% bovine serum albumin and 5% goat serum (from Jackson ImmunoResearch Laboratories, West Grove, PA). Islets were incubated in permeabilization solution supplemented with primary guinea pig anti-glucagon antibodies (1:500) for 24–48 h at 4 °C, washed with PBS three times, incubated with secondary anti-guinea pig antibodies conjugated with Alexa Fluor 488 (1:1000) and rabbit anti-GFP antibodies conjugated with Alexa Fluor 555 (1:250 from a stock of 2 mg/ml) for another 24–48 h, and washed three times before imaging. Alexa 488 and 555 were excited at 488 and 543 nm, and their emission was collected through a short (520–560 nm) and a long pass filter (>560 nm), respectively.

NAD(P)H Measurements—Islets were equilibrated in imaging buffer (as described above for flow sorting) at 1 mM glucose for 1 h. Islets were kept at 37 °C under 5% CO_2 using a temperature-controlled stage and objective warmer (Carl Zeiss Inc., Thornwood, NY). We used a two-photon excitation LSM710 laser-scanning microscope with a Fluar 40x/1.3NA oil immersion lens (Zeiss) to measure cellular redox state (33, 37, 38), using a Coherent Chameleon laser tuned to 710 nm (Coherent Inc., Santa Clara, CA). The laser power was kept below 3.5 milliwatts at the sample; at this laser power, no observable damage

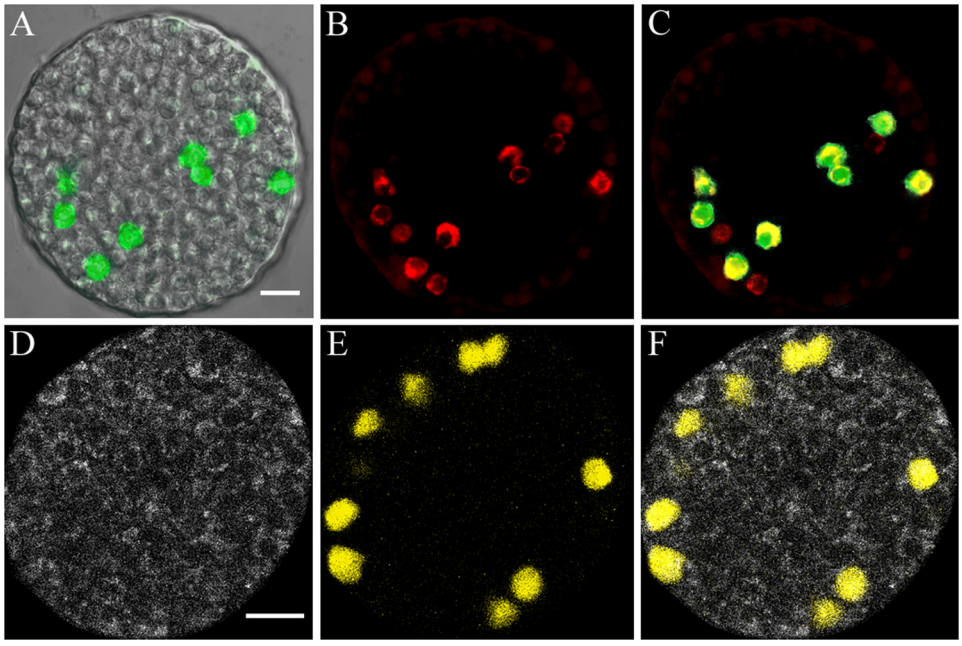

FIGURE 1. **Fluorescence-based visualization of α-cells within an islet.** *A,* overlay of differential interference contrast and anti-GFP antibody (*green*) images from a fixed permeabilized islet harvested from an EYFP-labeled α-cell animal. *B,* same islet stained with anti-glucagon antibodies (*red*). *C,* overlay of anti-GFP (*green*) and anti-glucagon (*red*) antibodies, co-localization presented in *yellow*. *D,* NAD(P)H autofluorescence signal of an islet perifused at 12 mM glucose. *E,* EYFP signal (*yellow*) emitted by α-cells within the islet presented in *D*. *F,* overlay of NAD(P)H and EYFP signals. *Scale bars,* 20 μm. *Bar* in *A* is valid for *A–C*. *Bar* in *D* is valid for *D* and *E*.

is caused to the islet (37). NAD(P)H fluorescence was collected by nondescanned detectors through a custom 380–500-nm filter (Chroma Inc., Rockingham, VT). Glucose concentrations were adjusted by addition of a preheated 100 mM stock solution at different locations on the edge of the imaging dish and mixed by gentle pipetting. Two-photon imaging was sequentially used with single-photon confocal imaging to localize the EYFP-expressing α-cells (pinhole diameter = 1.89 airy units). EYFP was excited at 514 nm, and the emission was collected through a 520–560 nm bandpass filter. For the dose-response curve at steady-state concentrations of glucose, a *z*-stack of an islet was acquired at 1 mM glucose, and another *z*-stack was collected 10 min after glucose stimulation, when NAD(P)H signal reaches a plateau. For a given α-cell, optical sections with the greatest EYFP fluorescence (*i.e.* the middle of the cell) were used as references for comparing NAD(P)H signals before and after glucose application. This strategy was used to overcome any cell movement. Non-EYFP cells were considered to represent β-cells.

Calcium Imaging—Islets were labeled with 10 μM FuraRed-AM or 5 μM Fluo4-AM for 1 h in imaging solution containing 1 mM glucose, at 37 °C. After washing, islets were allowed to equilibrate on the microscope stage for 15 min. FuraRed was used for measuring the calcium dose-response curve at steady-state concentrations of glucose. Sequential *z*-stack acquisitions of EYFP and FuraRed were performed as described previously. FuraRed was excited at 488 nm, and its fluorescence collected through a 620–680-nm bandpass filter. Controls for photobleaching and dye leakage out of the cells were performed on separate islets ($n = 7$) and showed no statistically significant decrease in FuraRed fluorescence ($-0.8 \pm 2\%$ for 19 α-cells and $0.06 \pm 3.69\%$ for β-cells). Time series Fluo4 imaging was used for recording calcium oscillations within RFP islets. Fluo4 was excited at 488 nm; its emission was recorded between 490 and 575 nm, and tdRFP was excited at 561 nm, and its fluorescence was collected between 538 and 735 nm (LSM710, Zeiss). Calcium concentration values can be approximated from single wavelength excitation of calcium dyes knowing the dissociation constant (K_D) of the probe and the basal calcium concentration (39, 40). The K_D values used for FuraRed and Fluo4 imaging were 1.1 and 0.35 μM, respectively (41, 42), and the basal calcium concentration was 80 nM in both α- and β-cells as estimated previously (43, 44).

Data Analysis and Statistics—Data were analyzed with Metamorph 7.6.1 (MDS Analytical Technologies, Downingtown, PA) and Excel 2007 (Microsoft, Redmond, WA). For analysis of single cells within islets, regions of interest were chosen to exclude cell edges to best ensure that none of the neighboring cell fluorescence was collected. Background signal was subtracted from all images analyzed. Statistical analyses and curve fittings were performed by Prism 4 (GraphPad Software, La Jolla, CA).

RESULTS

α-Cell Identification—Transgenic mice expressing fluorescent proteins in α-cells were obtained by breeding mice expressing Cre recombinase under control of the rat glucagon promoter (31, 32), with conditional reporter mice containing a loxP-flanked stop codon cassette between the ROSA26 promoter (45) and a fluorescent protein (EYFP or tdRFP) gene (32, 34). Immunocytochemistry shows that the expression of fluorescent proteins is specific to α-cells (Fig. 1). We found that ~63% of α-cells (132 of 210 cells), as determined by anti-glucagon antibodies, were labeled with fluorescent proteins (anti-GFP antibodies). All of the fluorescent protein-expressing cells are glucagon-positive, although 35–40% of the α-cells are not genetically labeled.

Hormone Secretion Assays—The glucose-dependent insulin and glucagon responses from EYFP-expressing islets are shown in Fig. 2*A*. As described by Quoix *et al.* (32), insulin and glucagon secretory responses to glucose are similar between wild-type and transgenic islets (data not shown). The results confirm that glucagon is mostly released at low glucose concentrations (<4 mM) when the release of insulin is minimal. Higher glucose levels (>7 mM) stimulate insulin secretion and inhibit glucagon release (Fig. 2*A*) (46–49). Even at higher glucose levels, however, α-cells retain an active secretory activity representing ~40% of the maximal response observed at low glucose. Application of arginine (10 mM), a potent glucagon secretagogue

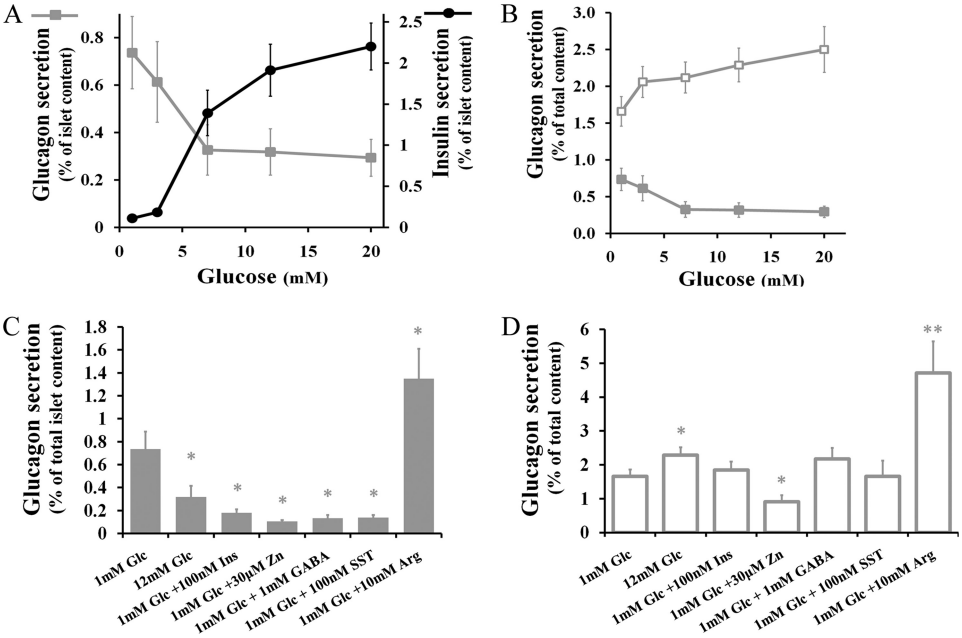

FIGURE 2. **Hormone secretion from intact islets and sorted α-cells.** *A,* percent of islet glucagon (*solid squares*) and insulin (*solid circles*) content secreted per h in response to glucose. When glucose levels are greater than or equal to 7 mM, both insulin and glucagon secretion are statistically different from base-line release at 1 mM ($n = 7$ islets, $p < 0.01$, ANOVA-independent samples). *B,* percent of glucagon content secreted from sorted α-cells (*open squares*) and intact islets (*solid squares*). Secretion from sorted cells is significantly greater at 12 and 20 mM than at 1 mM ($p < 0.05$, ANOVA). Between 14 and 30 assays were performed at any given glucose concentration. *C,* glucagon secretion responses from intact islets. *D,* glucagon secretion responses from flow-sorted α-cells. *Glc,* glucose; *Ins,* insulin; *SST,* somatostatin; *Arg,* arginine. *Error bars* represent the mean ± S.E. *, $p < 0.05$, **, $p < 0.01$, ANOVA.

(50), leads to an ~1.8-fold enhancement over basal glucagon release (from 0.74 ± 0.15%, $n = 7$, to 1.35 ± 0.26% of total cellular glucagon content, $n = 5$, $p < 0.05$, Student's t test, unpaired samples).

Although we were primarily interested in the behavior of α-cells in their native islet environment, the specific expression of EYFP within α-cells allows for efficient cell sorting by flow cytometry (fluorescence-activated cell sorting). Cells were sorted in the presence of propidium iodine, a viability dye, and cells positive for propidium iodine signal were excluded from the sorting. Post-sorting measurements of cell viability show that over 95% of sorted cells were viable, and these cells retain their ability to attach to gelatin-coated dishes for imaging purposes. Purity was determined to be >90% both by re-sorting samples of isolated cells and by counting the number of EYFP cells attached on the dishes after being cultured for 1 day. We also measured the insulin content in each assay and found no detectable traces of insulin. Glucagon secretion assays performed on these pure populations of α-cells show that glucagon secretion is 2-fold greater than that from intact islets at low glucose levels (1 mM) (Fig. 2*B*). Importantly, glucose does not inhibit glucagon secretion from isolated α-cells. Actually, glucose does stimulate glucagon release; application of 12 mM glucose increases basal secretion by 38.0 ± 3.8% ($n = 25$, $p < 0.05$, ANOVA). As it does in intact islets, arginine strongly stimulates glucagon secretion from sorted cells. Glucagon secretion at 1 mM glucose increases 2.8-fold after application of 10 mM arginine (from 1.66 ± 0.20%, $n = 30$, to 4.71 ± 0.9% of total cellular glucagon content, $n = 10$, $p < 0.001$).

Insulin, zinc ions, and GABA are released by β-cells (22–28) and somatostatin by δ-cells (29, 30, 51). All these compounds are candidate paracrine inhibitors of glucagon secretion from α-cells. We confirmed their inhibitory effects on glucagon secretion from intact islets incubated at 1 mM glucose (Fig. 2*C*). Application of 100 nM insulin, 30 μM zinc ions, 100 nM GABA, and 100 nM somatostatin reduces basal glucagon secretion by more than 75%. In comparison, an increase in glucose concentration to 12 mM inhibits the α-cell secretory activity by 56.8 ± 11.4%. We next investigated the effect of these inhibitors on flow-sorted α-cells. The same concentrations of insulin, GABA, and somatostatin had no significant effect on glucagon secretion (Fig. 2*D*). Interestingly, only zinc retained its inhibitory effect. The basal glucagon secretion was reduced by 45.2 ± 5.1% ($n = 17$, $p = 0.02$, Student's t test, unpaired samples).

α-Cell Glucose Metabolism Measured by Two-photon Excitation of NAD(P)H Autofluorescence—Glucose metabolism plays a pivotal role in insulin secretion. Less is known about the relationship between glucose utilization and glucagon release. Autofluorescence from reduced pyridine nucleotides (NADH and NADPH) can be used as an intrinsic probe to study cellular metabolism (52), because glucose metabolism leads to increased NAD(P)H autofluorescence. These changes in cellular redox potential can be measured quantitatively by two-photon excitation microscopy (33, 37, 38).

For intact islets, a step increase in glucose from 1 to 20 mM augments the intensity of islet NAD(P)H signals in both α- and β-cells (Fig. 3*A*). The time course of the NAD(P)H response is similar from both cell types and begins ~2 min after glucose application, reaching a plateau 30–60 s after the start of the response. The time series plot also illustrates the greater basal NAD(P)H-related signal measured at 1 mM glucose in α-cells compared with the rest of the islet (mostly β-cells). On average, the NAD(P)H autofluorescence intensity at 1 mM glucose was 40.8 ± 2.4% greater in α-cells than in β-cells ($n = 263$). To determine whether this greater basal signal could reflect a higher α-cell metabolic state at low glucose levels, we oxidized NADH by adding 1 μM of the mitochondrial uncoupler carbonyl cyanide 4-(trifluoromethoxy)phenylhydrazone (FCCP) (53). Addition of FCCP decreased the NADH autofluorescence signal intensity to the same extent in both α- and β-cells (−40.3 ± 3.1 and −38.0 ± 2.7%, respectively; $n = 19$, $p < 0.001$, Student's t test- paired samples). The α-cell autofluorescence intensity was still 38.5 ± 6.5% ($p < 0.001$) greater than in β-cells after NADH oxidation. Thus, this greater amount of α-cell

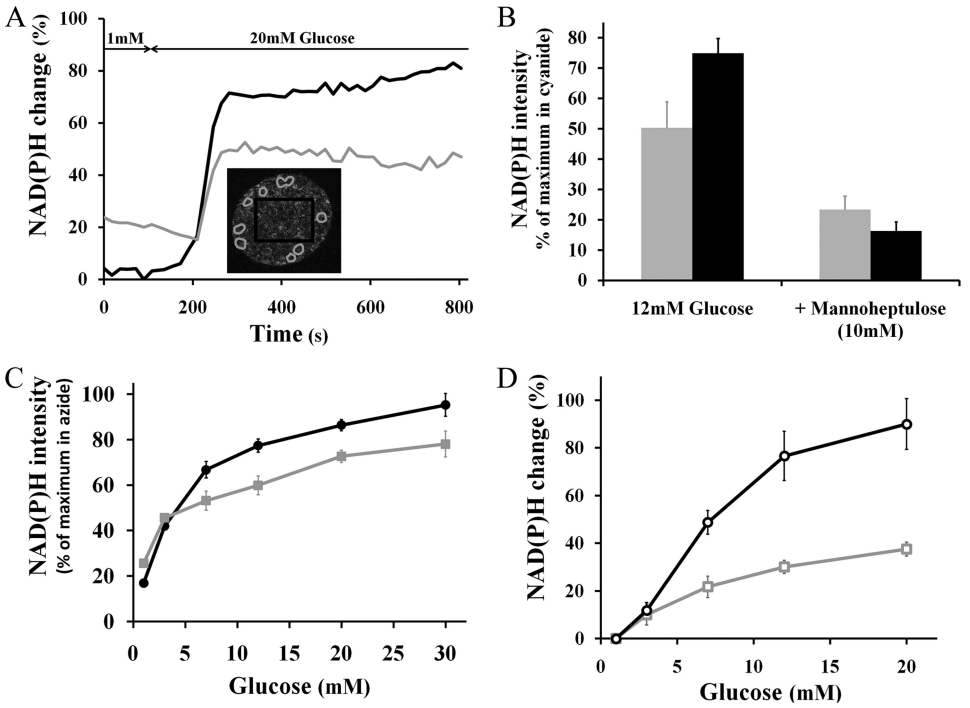

FIGURE 3. **Glucose-dependent NAD(P)H responses from intact islets and isolated cells.** *Black traces* indicate β-cells; *gray traces* indicate α-cells, both with S.E. *error bars*. *A,* representative time course of the NAD(P)H response from an islet exposed to a step increase in glucose from 1 to 20 mM; NAD(P)H emission was collected every 18 s. *Inset,* NAD(P)H islet image denotes α-cell locations by *gray circles* based on EYFP signal, and β-cell region of interest is shown by the *black rectangle*. *B,* normalized percent change in NAD(P)H response relative to base line (1 mM glucose). Application of 12 mM glucose increases cellular redox state in both α- and β-cells (*gray* and *black columns*, respectively). Addition of 10 mM D-mannoheptulose significantly inhibits NAD(P)H responses from both cell types ($p < 0.01$, $n = 12$ for α-cells and $n = 7$ for β-cells). *C,* normalized glucose dose-response curve of NAD(P)H from islet α-cells (*solid squares*, $n = 250$) and β-cells (*solid circles*, core regions averaged from 67 islets). *D,* % change in NAD(P)H autofluorescence to step increases in glucose from isolated α-cells compared with values at 1 mM glucose (*open squares*, $n = 146$) and isolated β-cells (*open circles*, $n = 269$). All NAD(P)H responses in *C* and *D* were significantly different from base line at 1 mM glucose ($p < 0.01$, ANOVA, independent samples).

autofluorescence collected through the NADH emission filter is likely due to non-NADH autofluorescence (*e.g.* elastin, collagen, and/or lipopigments). Assuming that FCCP fully oxidized NADH, we subtracted this "non-NADH" background to the autofluorescence intensity measured at 1 mM glucose. We found that the NAD(P)H base line was still 51.7 ± 6.2% ($p < 0.001$) greater in α-cells compared with β-cells.

The islet NAD(P)H response to step increases in glucose concentration (Fig. 3*C*) was normalized to the minimal NADH redox state obtained with FCCP and to the maximal signal following the application of sodium cyanide (3 mM). Cyanide blocks NADH oxidation by inhibiting the mitochondrial electron transport chain (53). Both α- and β-cells dose-dependently increased their NADH redox state with glucose. From 1 to 30 mM glucose, the dynamic range of the α-cell NAD(P)H response was ~2-fold less than for β-cells (3.1 ± 0.3 *versus* 5.7 ± 0.5, respectively). Fits of the glucose dose-response to a sigmoidal curve yielded an EC_{50} (half-maximal response) of 7.1 mM for α-cells (95% confidence interval, 1.3–39.2 mM) and 4.2 mM for β-cells (2.8–6.3 mM), which suggest that the metabolic response of both cell types is limited by glucokinase, a hexokinase with a low affinity for glucose (54). Application of a competitive inhibitor of glucokinase, D-mannoheptulose (10 mM) (55, 56), strongly reduces NAD(P)H autofluorescence in islets perifused at 12 mM glucose (Fig. 3*B*). The heptose was more potent at inhibiting β-cells than α-cells (78.2 ± 5.2% reduction in normalized β-cell NADH signal against 53.8 ± 8.9% inhibition for α-cells).

We also measured glucose dose-dependent increases in the NAD(P)H response from sorted α- and β-cells (Fig. 3*D*). The dynamic range of the α-cell response from the minimum obtained with FCCP to the maximum with cyanide is similar in both isolated cells and α-cells present in the islet (3.4 ± 0.3 for islet α-cells *versus* 3.1 ± 0.3 in isolated cells). Also, the dynamic range of the α-cell response to glucose is ~2-fold less than for β-cells, as found in islets. Fits of the glucose dose response to a sigmoidal curve yielded an EC_{50} of 8.4 mM for α-cells (confidence interval, 7.0–10.1 mM). As observed in dispersed β-cells (37), the NAD(P)H response to glucose was more heterogeneous from isolated α-cells than for those within intact islets. Only ~65% of isolated α-cells are responsive to glucose (at 12 and 20 mM) compared with over 95% of α-cells within intact islets. Also, the standard deviation of the increase from 1 to 12 mM glucose is greater in isolated α-cells (~70% of the mean compared with ~30% in islet α-cells).

α-Cell Free Calcium Activity in Response to Glucose—We measured the cytoplasmic calcium concentrations in EYFP-labeled α-cells using FuraRed-AM. In intact islets, both α- and β-cells respond to glucose by increasing their averaged $[Ca^{2+}]_i$ in a dose-dependent manner (Fig. 4*A*). Following the observed NAD(P)H response, the dynamic range of the calcium response is less in α-cells than in β-cells. For instance, a change in glucose from 1 to 12 mM augments α-cell $[Ca^{2+}]_i$ by 45.3 ± 5.3% and β-cell $[Ca^{2+}]_i$ by 96.0 ± 6.2%. We assessed the role of glucokinase for glucose-dependent increases in $[Ca^{2+}]_i$ by applying 10 mM of D-mannoheptulose to islets perifused with 12 mM glucose. Following treatment with the inhibitor, α-cell $[Ca^{2+}]_i$ was reduced by 19.5 ± 0.4% and β-cell $[Ca^{2+}]_i$ by 24.7 ± 0.9% (19 α-cells were analyzed from six islets, $p < 0.01$, Student's *t* test). Alternatively, we confirmed the stimulatory effect of 12 mM glucose on $[Ca^{2+}]_i$ by Fluo4 imaging on tdRFP islets incubated at 1 mM (+66.1 ± 3.2% for α-cells and +99.1 ± 12.6% for β-cells, 15 α-cells were analyzed from seven islets, $p < 0.01$, Student's *t* test). Overall, ~90% (48 of 54 cells) of α-cells within intact islets elevate their average $[Ca^{2+}]_i$ after switching the glucose concentration from 1 to 12 mM.

Blocking of the K_{ATP} channel with tolbutamide (57) increases α-cell calcium levels in intact islets. Addition of 100 μM tolbuta-

mide to the perifusion medium with 1 mM glucose leads to a 98.9 ± 10.7% augmentation of α-cell $[Ca^{2+}]_i$ as measured by FuraRed imaging (12 α-cells from three islets, $p < 0.01$, Student's *t* test, paired samples).

Sorted β-cells display a similar $[Ca^{2+}]_i$ response to glucose compared with β-cells in intact islets, as measured by FuraRed imaging (Fig. 4). However, the calcium response from isolated α-cells is considerably more heterogeneous. Over 50% of the cells exhibit a response similar to that seen within intact islets, but one-third of the cells show decreasing $[Ca^{2+}]_i$, and 10% of the isolated α-cells are not responsive.

α-Cell Calcium Oscillations in Response to Glucose and Other Glucagon Inhibitors—α-Cells are known to exhibit calcium activity at low glucose concentrations (43, 58–61). The specific expression of tdRFP in α-cells allows the use of Fluo4, a sensitive calcium indicator. At 1 mM glucose, 46% of islet α-cells (77 of 168 cells) were found to be oscillating during a 5-min observation period (Table 1). Calcium oscillations are also present at inhibitory concentrations of glucose (12 mM), with a similar proportion of oscillating cells (49%, 46 of 91 cells). Unlike the steady $[Ca^{2+}]_i$ oscillations seen in β-cells within intact islets, the α-cell calcium oscillations exhibit different shapes, amplitudes, and durations (Fig. 5, *A–C*) and random periodicity. Defining an oscillation as a local $[Ca^{2+}]_i$ peak in time with greater than a 15% change in Fluo4 signal, we calculated an overall frequency of 0.89 ± 0.07 oscillation/min from oscillating islet α-cells at 1 mM glucose. Interestingly, glucose application (12 mM) increases this frequency to 1.44 ± 0.18 oscillations/min ($p < 0.01$, Student's *t* test) but did not modify the amplitude distribution of the calcium events (Table 1). The time series of Fluo4 fluorescence is consistent with the averaged $[Ca^{2+}]_i$ changes reported with FuraRed described above. A representative time series of Fluo4 response (Fig. 5*C*) shows one α-cell that increases its oscillatory frequency after application of 7 mM glucose, and another responds by increasing its $[Ca^{2+}]_i$. Thus, calcium imaging of intact islets suggests that glucagon inhibition by glucose is not mediated by a decrease in calcium dynamics ($[Ca^{2+}]_i$ and oscillatory activity). We assessed the effect of candidate paracrine inhibitors of glucagon secretion on islet α-cell calcium oscillations and did not observe any significant change in their oscillatory behavior (Table 1).

The oscillatory activity of isolated α-cells showed that at 1 mM glucose, 53% exhibited calcium oscillations with the same frequency as α-cells present in intact islet (0.89 ± 0.1 oscillation/min). We did not observe any significant deviation in their oscillatory properties at elevated glucose levels or in the presence of zinc ions (Table 1).

As shown in Fig. 5*B*, calcium oscillations are not synchronized between adjacent α-cells ($n = 9$ adjacent pairs of oscillating α-cells). However, islet α-cell $[Ca^{2+}]_i$ does sometimes approximately follow the surrounding coordinated β-cell $[Ca^{2+}]_i$ waves (62) at glucose concentrations between 8 and 12 mM (18 of 25 α-cells, one representative example on Fig. 5*D*). However, the time course and duration of such α-cell signals show more complex oscillatory patterns compared with those in the β-cells (Fig. 5*D*). The α-cells signals are not likely to come from neighboring β-cells because of the following: 1) they do not always occur; 2) they follow a different time

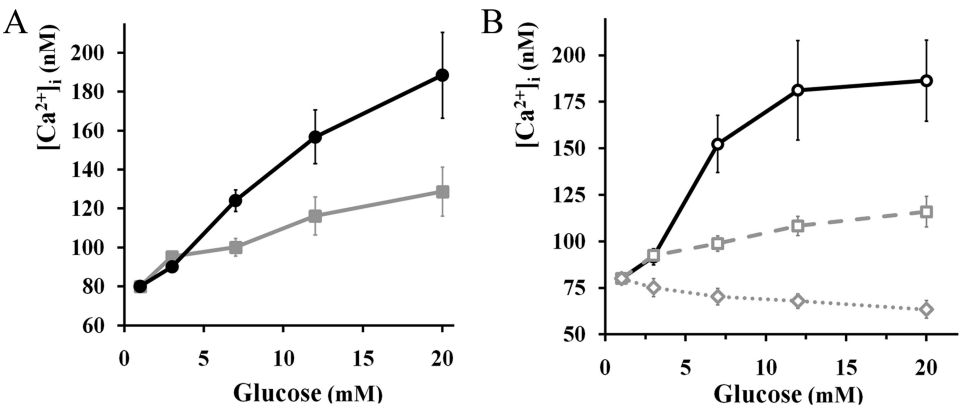

FIGURE 4. **Glucose-dependent changes in $[Ca^{2+}]_i$ by FuraRed imaging from intact islets and isolated cells.** *Black lines* and *gray lines* with S.E. *error bars* represent β- and α-cells, respectively. *A*, glucose-dependent $[Ca^{2+}]_i$ increases from intact islets. At glucose levels greater than or equal to 7 mM, changes were statistically significant to base line at 1 mM glucose ($n = 22$ α-cells from 7 islets, $p < 0.01$, ANOVA). *B*, glucose-dependent $[Ca^{2+}]_i$ changes from sorted cells. Two distinct responses were apparent from sorted α-cells. The *dashed gray line* represents α-cells responding to glucose by an increase in $[Ca^{2+}]_i$ (11 of 20 cells). The *dotted gray plot* indicates α-cells that decrease their $[Ca^{2+}]_i$ (7 of 20 cells). At glucose levels greater than or equal to 7 mM, changes were statistically significant from base line ($n = 9$ β-cells, $n = 20$ α-cells, $p < 0.01$, ANOVA, correlated samples).

TABLE 1

Comparison of α-cell calcium oscillation characteristics in response to glucose and inhibitors of glucagon secretion, as measured by Fluo4 imaging

Each α-cell was monitored during 5 min for each condition.

	No. of cells analyzed	% of oscillating cells	Frequency (oscillations/min)	Amplitude of oscillations		
				+15–30% increase	+30–60%	>60%
				%	%	%
Islets at 1 mM glucose	168	46	0.89 ± 0.07	56.1 ± 5.6	28.8 ± 3.7	15.1 ± 3.5
Islets at 12 mM glucose	91	49	1.44 ± 0.18[a]	52.4 ± 7.1	30.8 ± 5.3	16.8 ± 5.2
Islets at 1 mM glucose + 100 nM insulin	60	45	0.71 ± 0.09	63.0 ± 11.8	21.7 ± 6.9	15.2 ± 7.2
Islets at 1 mM glucose + 30 μM zinc	62	40	0.84 ± 0.17	56.4 ± 12.8	30.8 ± 9.7	12.8 ± 5.7
Islets at 1 mM glucose + 1 mM GABA	57	39	0.84 ± 0.14	55.7 ± 13.4	27.3 ± 6.4	17.0 ± 7.7
Islets at 1 mM glucose + 100 nM somatostatin	46	50	0.78 ± 0.09	60.9 ± 8.1	30.5 ± 8.4	8.6 ± 2.9
Isolated cells at 1 mM	45	53	0.89 ± 0.10	55.5 ± 6.6	25.6 ± 6.3	18.9 ± 5.6
Isolated cells at 12 mM	52	52	0.97 ± 0.15	64.5 ± 8.9	20.7 ± 5.3	14.9 ± 6.9
Isolated cells at 1 mM + 30 μM zinc	30	57	0.67 ± 0.10	75.0 ± 13.1	20.3 ± 7.2	4.7 ± 2.6

[a] $p < 0.01$, unpaired Student's *t* test, as compared with 1 mM glucose.

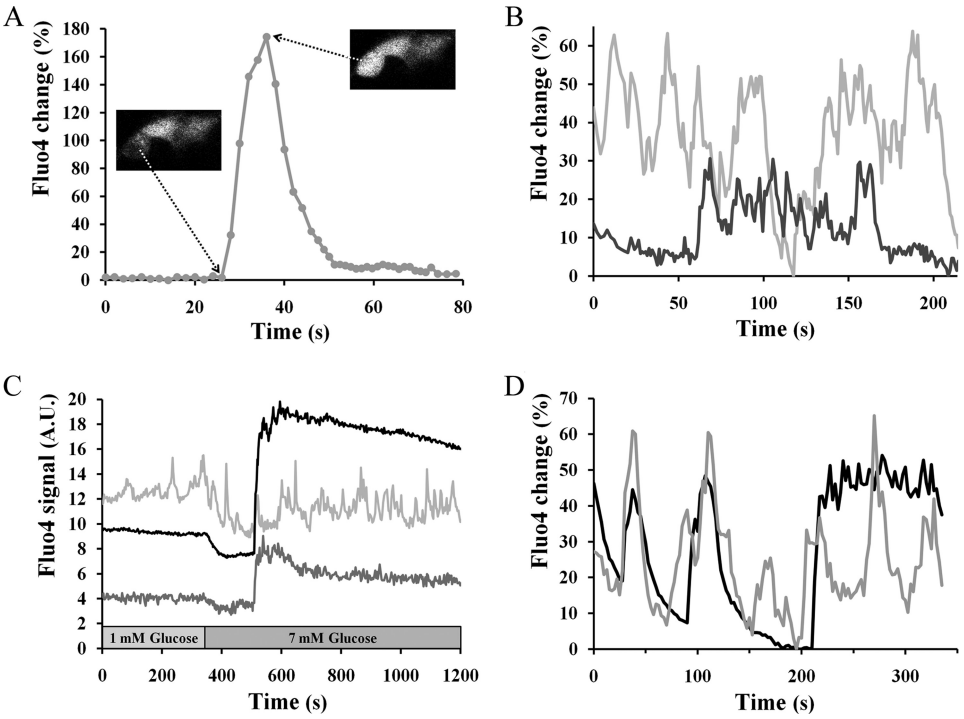

FIGURE 5. **Calcium oscillations from α-cells within intact islets as measured by Fluo4.** *A, B,* and *D* are time series of the Fluo4 signal relative to the minimal intensity recorded during the experiment. *A,* single calcium pulse from one islet α-cell perifused with 1 mM glucose. The *inset* images show the cell before and at the maximum of the calcium transient. *B,* two adjacent α-cells within an islet exposed to 1 mM glucose show no synchronization between their $[Ca^{2+}]_i$ responses. *C,* representative time course of the Fluo4 response from an islet exposed to a step increase in glucose from 1 to 7 mM. The *black line* indicates a region of β-cells, and the *gray plots* show the responses of two individual α-cells. Fluo4 signal was recorded every 2 s. *D,* representative time course of Fluo4 signals from an islet exposed to 12 mM glucose. The *black line* indicates β-cells, and the *gray line* represents an α-cell. Fluo4 signal was recorded every 2.5 s, and the confocal pinhole diameter was 1 airy unit.

course when they do occur; and 3) there was no change in their properties as the confocal pinhole diameter was decreased down to 1 airy unit, where any out-of-focus fluorescence from beyond a couple of micrometers would be totally rejected (63).

DISCUSSION

A major impediment in the study of α-cells has been the lack of reliable methods to identify them within the intact islet. Previous research has been based on post hoc immunostaining analyses (58–61, 64–66), electrophysiological characteristics (17, 18, 67), or cell sorting based on size and autofluorescence (16, 23, 24, 50, 68). It is challenging to trace a single cell within an intact islet before and after immunostaining treatment because of the morphological changes that inevitably follow tissue fixation. Electrophysiological identification can degenerate given the variability of reported electrical properties of different islet cell types (69). Sorting by size or by autofluorescence yields significant overlap of different cell types and does not discriminate well between α- and other non-β-cells (68). Sorting has only been applied on rat cells (16, 23, 24, 50, 68), but the availability of transgenic mice that specifically express fluorescent proteins in α-cells allows for easy and precise identification (Fig. 1). It is therefore possible to study them both within intact islets and in dispersed cell populations. Hormone secretion assays indicate that the intact pancreatic islet is a good model for studying the mechanisms of glucagon suppression by glucose. Glucagon release from islets is indeed maximal at low glucose levels and inhibited at increasing concentrations of glucose (Fig. 2*A*), similar to *in vivo* measurements (48).

Comparison of Glucagon Secretion between Intact Mouse Islets and Isolated α-Cells—To separate paracrine inhibition from possible direct suppressive effects of glucose, we studied the secretory responses of pure populations of isolated mouse α-cells. Flow-sorted α-cells are viable, and arginine retains its ability to stimulate glucagon secretion. However, important differences emanate from the comparison with α-cells present in intact islets. First, at basal glucose concentration (1 mM), isolated cells secrete ~2-fold more glucagon than do cells within intact islets. This greater basal secretion has been also reported in dispersed rat islets and flow-sorted rat α-cells (68–71) and suggests that even base-line α-cell secretory activity is tonically inhibited in the islet. This observation emphasizes the importance of cell-cell contacts (juxtacrine signaling) or paracrine effectors for normal glucagon response. Second, glucose does not inhibit the glucagon secretion from α-cells removed from the islet environment. In fact, glucose has a stimulatory effect on isolated mouse α-cells (Fig. 2*B*). The lack of inhibition of glucagon secretion from pure populations of α-cells argues against a direct suppressive action of glucose and supports a paracrine model.

We therefore investigated the effects of the candidate paracrine inhibitors, insulin, GABA, zinc ions, and somatostatin. All of these inhibited glucagon secretion from intact islets (Fig. 2*A*). However, only zinc retains its ability to inhibit glucagon secretion from pure populations of mouse α-cells (Fig. 2*B*). These results support previous studies on isolated rat α-cells (23, 24) describing a stimulatory effect for both glucose and arginine and an inhibitory effect for zinc. Overall, our hormone assays indicate that α-cells behave quite differently when they are retrieved from their intra-islet milieu and that it is not possible to extrapolate from isolated cells to the islet behavior. These differences in glucagon secretion could originate from loss of juxtacrine or paracrine signals. However, the loss of response to insulin, GABA, and somatostatin from isolated cells is puzzling but might arise from proteolytic damage during cell dispersion and from loss of cell-cell contacts (72).

Glucose-dependent Metabolic Responses—β-Cell glucose metabolism plays a pivotal role in insulin secretion (6–13). In contrast, the role of α-cell in glucagon secretion remains to be determined. Biochemical approaches report glucose-dependent increases in the rates of glucose oxidation (14, 73–75) and

greater ATP to ADP ratios (22, 25, 76). However, previous attempts to measure any changes in α-cell NAD(P)H or flavoprotein autofluorescence by single-photon excitation have been unsuccessful (32, 66, 77, 78). The conjunction of two-photon excitation of NAD(P)H autofluorescence and fluorescence-based identification of mouse α-cells rendered possible the dynamic measurement of their metabolic redox state (Fig. 3). The NAD(P)H response to glucose indicates a dose-dependent metabolism in α-cells. NAD(P)H levels measured in islets incubated at 1 mM glucose were ~50% greater in α-cells than in β-cells. This enhanced metabolic redox state is consistent with greater basal α-cell ATP to ADP ratio (75) and likely illustrates the metabolic potential needed for maximal glucagon secretion at low glucose levels. From 1 to 30 mM glucose, the NAD(P)H levels were increased ~3-fold in α-cells and ~6-fold in β-cells. The reduced dynamic range in α-cells is in agreement with previous studies reporting lower glucose oxidation rates and ATP/ADP ratios as compared with β-cells (22, 73–75). Glucokinase is an allosteric enzyme that displays a sigmoidal steady-state kinetic response toward increasing glucose concentrations in the millimolar range. Glucokinase is established as the rate-limiting step for β-cell glycolysis (7), and NAD(P)H response to glucose follows glucokinase kinetics (Fig. 3*C*) (37). Glucokinase is also expressed in α-cells (15), and the time course of the α-cell NAD(P)H response, EC_{50}, and inhibition by glucokinase inhibitor (D-mannoheptulose) suggest that glucokinase is also the rate-limiting step for α-cell glycolysis (Fig. 3). The half-maximal glucose response obtained from islet α-cells is slightly right-shifted as compared with β-cells (7 and 4 mM, respectively) and could reflect cell-specific differences in the regulation of glucokinase.

The inhibition of glucagon secretion from intact islets occurs between 3 and 7 mM glucose (Fig. 2*A*), but α-cell metabolic redox state only augments by 16.4 ±1.4% (Fig. 3*C*) at the same time. It seems unlikely that such a small change in metabolism accounts for the suppressive effect of glucose observed in islets.

Cytoplasmic Calcium Responses—Influx of calcium ions is a trigger for exocytosis of endocrine vesicles, and the amount of insulin secreted from normal β-cells is closely related to $[Ca^{2+}]_i$ (Figs. 2 and 4) (11–13). Because glucagon release from islets is inhibited at elevated concentrations of glucose (Fig. 2*A*), one would naively expect the α-cell $[Ca^{2+}]_i$ to drop concomitantly. Several models of glucose-mediated suppression of glucagon secretion rely on this assumption; however, there is poor consensus regarding glucose-mediated calcium dynamics in the α-cell. Some studies report a decrease in cytoplasmic calcium levels or a slowing down of oscillation frequencies in response to glucose (59–61), and some report a weak or negligible effect (25, 79), although some others describe glucose-mediated increases in $[Ca^{2+}]_i$ (24, 58). Our calcium measurements on intact islets (FuraRed and Fluo4 imaging) indicate that α-cells respond to glucose by elevating their averaged $[Ca^{2+}]_i$ (Figs. 4*A* and 5*C*). The extent of the response is ~50% less than in β-cells (from 1 to 12 mM glucose) and can be inhibited by D-mannoheptulose. Application of the K_{ATP} channel blocker tolbutamide also increases α-cell calcium levels. Together, these results suggest that the same mechanism may be responsible for both α- and β-cell calcium increases to glucose; glycolysis, increased ATP/ADP, K_{ATP} closure, membrane depolarization, and activation of voltage-gated calcium channels, as has been proposed previously (24).

In contrast to intact islets, $[Ca^{2+}]_i$ responses to glucose from isolated α-cells are more diverse; ~50% respond similarly to α-cells in intact islets, and ~50% of these are either nonresponsive or slightly decrease their $[Ca^{2+}]_i$ (Fig. 4*B*). To a lesser extent, this pronounced heterogeneity was also seen in the metabolic responses. Our experiments indicate that α-cells removed from the islet behave quite differently in terms of their NAD(P)H, calcium, and secretory responses. In other words, α-cells need the three-dimensional cytoarchitecture of the islet for normal physiology. Deviations in isolated α-cell response could be attributed to loss of cell-cell contacts, loss of paracrine communication, or proteolytic damage during islet dispersion (68–72). Most research on α-cell biology to date has been conducted on isolated cells. Besides the possible artifacts coming from the difficulty to distinguish these cells from other cell types, part of the controversy on α-cell metabolic and calcium responses could originate from the wide heterogeneity found in isolated cells. Our data show that α-cells within intact islets provide a much more physiologically relevant and robust approach to investigate these cells.

One noticeable difference between α- and β-cell calcium responses is their oscillatory pattern. α-Cells exhibit apparently random, asynchronous calcium oscillations at low glucose levels, whereas β-cells display regular and synchronous calcium waves at higher glucose concentrations (>7 mM) (62). We measured these oscillations in labeled α-cells in intact islets and found the same proportion of oscillating α-cells at low and high glucose levels (Table 1). Although the shape and amplitude distribution of $[Ca^{2+}]_i$ signals do not depend on glucose, the oscillating cells do display greater frequencies at high glucose level. Taken together, these results indicate that inhibition of glucagon secretion from intact islets is not mediated by a decrease in calcium levels or slowing down of oscillations.

Few studies relate the effects of glucagon inhibitors on α-cell $[Ca^{2+}]_i$. One study on dispersed mouse α-cells reports a slight decrease, if any, in $[Ca^{2+}]_i$ following the addition of insulin, and no change in calcium signal was observed with zinc or GABA (79). Insulin was found to inhibit calcium signals in a clonal α-cell line, but the effect was lost at glucose levels above 1 mM (25). In addition, it was found that somatostatin does not reduce $[Ca^{2+}]_i$ in sorted rat α-cells (80) and that zinc slightly stimulates the frequency of calcium oscillations in dispersed mouse α-cells and in a clonal α-cell line (25). Our calcium measurements from intact mouse islets demonstrate that application of the candidate paracrine inhibitors of glucagon secretion, insulin, zinc, GABA, and somatostatin, does not significantly affect the α-cell intracellular calcium dynamics. Consequently, the suppressive effect of glucose is likely to act downstream from α-cell Ca^{2+} signals, presumably at the vesicle trafficking or exocytotic machinery level. For instance, glucagon inhibition could be mediated by a reduced likelihood of granule fusion with the plasma membrane, by depriming of docked vesicles, or by a depletion of the readily releasable pool of glucagon-containing vesicles. Very few studies provide information on the mechanisms of α-cell granule trafficking and

exocytosis. Nonetheless, inhibition of glucagon secretion by somatostatin has been shown to involve a $G\alpha_{i2}$ protein-dependent pathway where activation of the protein phosphatase calcineurin leads to depriming of docked secretory granules belonging to the readily releasable pool (80). In that case, no decrease in $[Ca^{2+}]_i$ was observed. Furthermore, it has been reported that the size of the readily releasable pool is tightly regulated and depends on cAMP levels. Adrenaline, via cAMP elevation, mediates its stimulatory effect on glucagon secretion by enhancing up to 5-fold the rate of granule mobilization from a reserve pool (18). Unraveling the precise secretory mechanisms responsible for glucose-stimulated glucagon inhibition in intact islets will require further investigations.

α-/β-Cell Synchronization during Whole Islet Calcium Waves—Intracellular calcium oscillations are not coordinated between adjacent α-cells in islets perifused at low glucose levels (Fig. 5*B*). However, α-cells exhibit some synchronization with β-cells during the regular synchronous calcium waves seen between 7 and 12 mM (Fig. 5*D*). The spreading of $[Ca^{2+}]_i$ waves into α-cells likely contributes to the greater $[Ca^{2+}]_i$ measured at high glucose (Fig. 4*A*). Intercellular communication through gap junctions made of connexin-36 is the consensus explanation behind the generation of periodic β-cell calcium waves and concomitant insulin pulses (51, 62, 81). Whether gap junctions are present in α-cell membrane is still a matter of debate (65, 82) but the observed α-/β-cell synchrony during calcium waves seems to hint that gap junctions might also connect these two cell types.

Acknowledgments—Glucagon-Cre mice were generously provided by Dr. Pedro Herrera (Department of Genetic Medicine and Development, University of Geneva, Geneva, Switzerland). We thank Dr. Hervé Luche and Dr. Hans Jörg Fehling for their gift of ROSA26-tdRFP mice (Institute of Immunology, University Clinics Ulm, Ulm, Germany), distributed through the European Mouse Mutant Archive, and Dr. Alvin Powers for providing us with ROSA26-EYFP mice (Department of Medicine, Vanderbilt University, Nashville, TN). Equipment and technical assistance was provided by the Vanderbilt Hormone Assay and Flow Sorting Core Laboratories and was supported by National Institutes of Health Grant DK20593 to the Vanderbilt Diabetes Center, National Institutes of Health Grant CA68485 to Vanderbilt Ingram Cancer Center, and National Institutes of Health Grant DK58404 to the Vanderbilt Digestive Disease Research Center.

REFERENCES

1. Unger, R. H. (1981) *Diabetologia* **20,** 1–11
2. Wierup, N., Svensson, H., Mulder, H., and Sundler, F. (2002) *Regul. Pept.* **107,** 63–69
3. Jiang, G., and Zhang, B. B. (2003) *Am. J. Physiol. Endocrinol. Metab.* **284,** E671–E678
4. Matsuda, M., Defronzo, R. A., Glass, L., Consoli, A., Giordano, M., Bressler, P., and Delprato, S. (2002) *Metabolism* **51,** 1111–1119
5. Cryer, P. E., Davis, S. N., and Shamoon, H. (2003) *Diabetes Care* **26,** 1902–1912
6. Hughes, S. D., Quaade, C., Johnson, J. H., Ferber, S., and Newgard, C. B. (1993) *J. Biol. Chem.* **268,** 15205–15212
7. Matschinsky, F. M. (1990) *Diabetes* **39,** 647–652
8. De Vos, A., Heimberg, H., Quartier, E., Huypens, P., Bouwens, L., Pipeleers, D., and Schuit, F. (1995) *J. Clin. Invest.* **96,** 2489–2495
9. Cook, D. L., and Hales, C. N. (1984) *Nature* **311,** 271–273
10. Detimary, P., Van den Berghe, G., and Henquin, J. C. (1996) *J. Biol. Chem.* **271,** 20559–20565
11. Wollheim, C. B., and Sharp, G. W. (1981) *Physiol. Rev.* **61,** 914–973
12. Hoenig, M., and Sharp, G. W. (1986) *Endocrinology* **119,** 2502–2507
13. Satin, L. S., and Cook, D. L. (1985) *Pflugers Arch.* **404,** 385–387
14. Heimberg, H., De Vos, A., Pipeleers, D., Thorens, B., and Schuit, F. (1995) *J. Biol. Chem.* **270,** 8971–8975
15. Heimberg, H., De Vos, A., Moens, K., Quartier, E., Bouwens, L., Pipeleers, D., Van Schaftingen, E., Madsen, O., and Schuit, F. (1996) *Proc. Natl. Acad. Sci. U.S.A.* **93,** 7036–7041
16. Bokvist, K., Olsen, H. L., Høy, M., Gotfredsen, C. F., Holmes, W. F., Buschard, K., Rorsman, P., and Gromada, J. (1999) *Pflugers Arch.* **438,** 428–436
17. Göpel, S. O., Kanno, T., Barg, S., Weng, X. G., Gromada, J., and Rorsman, P. (2000) *J. Physiol.* **528,** 509–520
18. Gromada, J., Bokvist, K., Ding, W. G., Barg, S., Buschard, K., Renström, E., and Rorsman, P. (1997) *J. Gen. Physiol.* **110,** 217–228
19. Vignali, S., Leiss, V., Karl, R., Hofmann, F., and Welling, A. (2006) *J. Physiol.* **572,** 691–706
20. Gromada, J., Ma, X., Høy, M., Bokvist, K., Salehi, A., Berggren, P. O., and Rorsman, P. (2004) *Diabetes* **53,** Suppl. 3, S181–S189
21. Liu, Y. J., Vieira, E., and Gylfe, E. (2004) *Cell Calcium* **35,** 357–365
22. Ishihara, H., Maechler, P., Gjinovci, A., Herrera, P. L., and Wollheim, C. B. (2003) *Nat. Cell Biol.* **5,** 330–335
23. Franklin, I., Gromada, J., Gjinovci, A., Theander, S., and Wollheim, C. B. (2005) *Diabetes* **54,** 1808–1815
24. Olsen, H. L., Theander, S., Bokvist, K., Buschard, K., Wollheim, C. B., and Gromada, J. (2005) *Endocrinology* **146,** 4861–4870
25. Ravier, M. A., and Rutter, G. A. (2005) *Diabetes* **54,** 1789–1797
26. Rorsman, P., Berggren, P. O., Bokvist, K., Ericson, H., Möhler, H., Ostenson, C. G., and Smith, P. A. (1989) *Nature* **341,** 233–236
27. Wendt, A., Birnir, B., Buschard, K., Gromada, J., Salehi, A., Sewing, S., Rorsman, P., and Braun, M. (2004) *Diabetes* **53,** 1038–1045
28. Xu, E., Kumar, M., Zhang, Y., Ju ,W., Obata, T., Zhang, N., Liu, S., Wendt, A., Deng, S., Ebina, Y., Wheeler, M. B., Braun, M., and Wang, Q. (2006) *Cell Metab.* **3,** 47–58
29. Cejvan, K., Coy, D. H., and Efendic, S. (2003) *Diabetes* **52,** 1176–1181
30. Hauge-Evans, A. C., King, A. J., Carmignac, D., Richardson, C. C., Robinson, I. C., Low, M. J., Christie, M. R., Persaud, S. J., and Jones, P. M. (2009) *Diabetes* **58,** 403–411
31. Herrera, P. L. (2000) *Development* **127,** 2317–2322
32. Quoix, N., Cheng-Xue, R., Guiot, Y., Herrera, P. L., Henquin, J. C., and Gilon, P. (2007) *FEBS Lett.* **581,** 4235–4240
33. Bennett, B. D., Jetton, T. L., Ying, G., Magnuson, M. A., and Piston, D. W. (1996) *J. Biol. Chem.* **271,** 3647–3651
34. Luche, H., Weber, O., Nageswara Rao, T., Blum, C., and Fehling, H. J. (2007) *Eur. J. Immunol.* **37,** 43–53
35. Hara, M., Wang, X., Kawamura, T., Bindokas, V. P., Dizon, R. F., Alcoser, S. Y., Magnuson, M. A., and Bell, G. I. (2003) *Am. J. Physiol. Endocrinol. Metab.* **284,** E177–E183
36. Lacy, P. E., and Kostianovsky, M. (1967) *Diabetes* **16,** 35–39
37. Piston, D. W., and Knobel, S. M. (1999) *Methods Enzymol.* **307,** 351–368
38. Patterson, G. H., Knobel, S. M., Arkhammar, P., Thastrup, O., and Piston, D. W. (2000) *Proc. Natl. Acad. Sci. U.S.A.* **97,** 5203–5207
39. Grynkiewicz, G., Poenie, M., and Tsien, R. Y. (1985) *J. Biol. Chem.* **260,** 3440–3450
40. Cannell, M. B., Cheng, H., and Lederer, W. J. (1994) *Biophys. J.* **67,** 1942–1956
41. Kurebayashi, N., Harkins, A. B., and Baylor, S. M. (1993) *Biophys. J.* **64,** 1934–1960
42. Gee, K. R., Brown, K. A., Chen, W. N., Bishop-Stewart, J., Gray, D., and Johnson, I. (2000) *Cell Calcium* **27,** 97–106
43. Berts, A., Ball, A., Gylfe, E., and Hellman, B. (1996) *Biochim. Biophys. Acta* **1310,** 212–216
44. Gilon, P., and Henquin, J. C. (1992) *J. Biol. Chem.* **267,** 20713–20720
45. Soriano, P. (1999) *Nat. Genet.* **21,** 70–71
46. Unger, R. H. (1971) *N. Engl. J. Med.* **285,** 443–449

47. Vieira, E., Salehi, A., and Gylfe, E. (2007) *Diabetologia* **50,** 370–379
48. Shiota, C., Rocheleau, J. V., Shiota, M., Piston, D. W., and Magnuson, M. A. (2005) *Am. J. Physiol. Endocrinol. Metab.* **289,** E570–E577
49. MacDonald, P. E., De Marinis, Y. Z., Ramracheya, R., Salehi, A., Ma, X., Johnson, P. R., Cox, R., Eliasson, L., and Rorsman, P. (2007) *PLoS Biol.* **5,** e143
50. Pipeleers, D. G., Schuit, F. C., Van Schravendijk, C. F., and Van de Winkel, M. (1985) *Endocrinology* **117,** 817–823
51. Ravier, M. A., Güldenagel, M., Charollais, A., Gjinovci, A., Caille, D., Söhl, G., Wollheim, C. B., Willecke, K., Henquin, J. C., and Meda, P. (2005) *Diabetes* **54,** 1798–1807
52. Barlow, C. H., and Chance, B. (1976) *Science* **193,** 909–910
53. Eng, J., Lynch, R. M., and Balaban, R. S. (1989) *Biophys. J.* **55,** 621–630
54. Magnuson, M. A., and Matschinsky, F. M. (2004) *Front. Diabetes* **16,** 1–17
55. Coore, H. G., and Randle, P. J. (1964) *Biochem. J.* **91,** 56–59
56. Sweet, I. R., Li, G., Najafi, H., Berner, D., and Matschinsky, F. M. (1996) *Am. J. Physiol.* **271,** E606–E625
57. Proks, P., Reimann, F., Green, N., Gribble, F., and Ashcroft, F. (2002) *Diabetes* **51,** Suppl. 3, S368–S376
58. Asada, N., Shibuya, I., Iwanaga, T., Niwa, K., and Kanno, T. (1998) *Diabetes* **47,** 751–757
59. Nadal, A., Quesada, I., and Soria, B. (1999) *J. Physiol.* **517,** 85–93
60. Quesada, I., Nadal, A., and Soria, B. (1999) *Diabetes* **48,** 2390–2397
61. Quesada, I., Todorova, M. G., Alonso-Magdalena, P., Beltrá, M., Carneiro, E. M., Martin, F., Nadal, A., and Soria, B. (2006) *Diabetes* **55,** 2463–2469
62. Benninger, R. K., Zhang, M., Head, W. S., Satin, L. S., and Piston, D. W. (2008) *Biophys. J.* **95,** 5048–5061
63. Sandison, D. R., Piston, D. W., Williams, R. M., and Webb, W. W. (1995) *Appl. Optics* **34,** 3576–3588
64. Michaels, R. L., and Sheridan, J. D. (1981) *Science* **214,** 801–803
65. Meda., P., Santos, R. M., and Atwater, I. (1986) *Diabetes* **35,** 232–236
66. Quesada, I., Todorova, M. G., and Soria, B. (2006) *Biophys. J.* **90,** 2641–2650
67. Göpel, S., Zhang, Q., Eliasson, L., Ma, X. S., Galvanovskis, J., Kanno, T., Salehi, A., and Rorsman, P. (2004) *J. Physiol.* **556,** 711–726
68. Fletcher, D. J., Grogan, W. M., Barras, E., and Weir, G. C. (1983) *Endocrinology* **113,** 1791–1798
69. Gromada, J., Franklin, I., and Wollheim, C. B. (2007) *Endocr. Rev.* **28,** 84–116
70. Weir, G. C., Halban, P. A., Meda, P., Wollheim, C. B., Orci, L., and Renold, A. E. (1984) *Metabolism* **33,** 447–453
71. Weir, G. C., Leahy, J. L., Barras, E., and Braunstein, L. P. (1986) *Horm. Res.* **24,** 62–72
72. Konstantinova, I., Nikolova, G., Ohara-Imaizumi, M., Meda, P., Kucera, T., Zarbalis, K., Wurst, W., Nagamatsu, S., and Lammert, E. (2007) *Cell* **129,** 359–370
73. Gorus, F. K., Malaisse, W. J., and Pipeleers, D. G. (1984) *J. Biol. Chem.* **259,** 1196–1200
74. Schuit, F., De Vos, A., Farfari, S., Moens, K., Pipeleers, D., Brun, T., and Prentki, M. (1997) *J. Biol. Chem.* **272,** 18572–18579
75. Detimary, P., Dejonghe, S., Ling, Z., Pipeleers, D., Schuit, F., and Henquin, J. C. (1998) *J. Biol. Chem.* **273,** 33905–33908
76. Ostenson, C. G. (1979) *Diabetologia* **17,** 325–330
77. Mercan, D., Kadiata, M. M., and Malaisse, W. J. (1999) *Biochem. Biophys. Res. Commun.* **262,** 346–349
78. Martens, G. A., Cai, Y., Hinke, S., Stangé, G., Van de Casteele, M., and Pipeleers, D. (2005) *J. Biol. Chem.* **280,** 20389–20396
79. Quoix, N., Cheng-Xue, R., Mattart, L., Zeinoun, Z., Guiot, Y., Beauvois, M. C., Henquin, J. C., and Gilon, P. (2009) *Diabetes* **58,** 412–421
80. Gromada, J., Høy, M., Buschard, K., Salehi, A., and Rorsman, P. (2001) *J. Physiol.* **535,** 519–532
81. Rocheleau, J. V., Remedi, M. S., Granada, B., Head, W. S., Koster, J. C., Nichols, C. G., and Piston, D. W. (2006) *PLoS Biol.* **4,** e26
82. Göpel, S., Kanno, T., Barg, S., Galvanovskis, J., and Rorsman, P. (1999) *J. Physiol.* **521,** 717–728